PHYSICAL REVIEW D **96,** 063516 (2017)

Parametrizing modified gravity for cosmological surveys

Jérôme Gleyzes

Jet Propulsion Laboratory, California Institute of Technology, Pasadena 91109, California
and California Institute of Technology, Pasadena 91125, California

(Received 12 June 2017; published 15 September 2017)

One of the challenges in testing gravity with cosmology is the vast freedom opened when extending General Relativity. For linear perturbations, one solution consists in using the effective field theory of dark energy. Even then, the theory space is described in terms of a handful of free functions of time. This needs to be reduced to a finite number of parameters to be practical for cosmological surveys. We explore in this article how well simple parametrizations, with a small number of parameters, can fit observables computed from complex theories. Imposing the stability of linear perturbations appreciably reduces the theory space we explore. We find that observables are not extremely sensitive to short time-scale variations and that simple, smooth parametrizations are usually sufficient to describe this theory space. Using the Bayesian information criterion, we find that using two parameters for each function (an amplitude and a power-law index) is preferred over complex models for 86% of our theory space.

DOI: 10.1103/PhysRevD.96.063516

I. INTRODUCTION

With many large scale structure surveys, such as WFIRST [1], LSST [2], DESI [3], SPHEREx [4], and EUCLID [5], coming online in the close future, our chances of understanding what is causing the accelerated expansion of the Universe are improving drastically. While a cosmological constant is still consistent with the data, it is informative to see how deviations from our standard cosmological model Lambda Cold Dark Matter(ΛCDM) could be constrained with these upcoming experiments.

It was shown in the broad framework of the effective field theory of dark energy (EFT of DE) [6–8] that to describe modifications of gravity involving a single extra degree of freedom (DOF), such as a scalar field, only five free functions of time are needed.[1] In particular, they can be used to describe known models such as Horndeski theories [10] and their extensions [11–13]. The case of Horndeski only requires four out of the five functions of time, and they have been expressed in an insightful and convenient way in Ref. [14]. The addition of beyond Horndeski theories to the notation of Ref. [14] was presented in Ref. [15]. Note that, recently, the formalism was extended to include also the possibility of modifications of gravity including additional vectors and tensors [16,17].

When used in the context of a specific model, these functions of time are not free but can be computed once the parameters of said model are given. Doing so requires solving the background equations to get the associated time evolution so that in principle the EFT of DE can be used as a proxy for specific models. However, no clear candidate stands out as a promising alternative to General Relativity (GR), which means that one should probably not focus only on these models.

The EFT of DE then becomes particularly critical; there is no need to specify a given model, since the appearance of these five functions of time arises generically when allowing the presence of a scalar field. The framework allows one to thoroughly and systematically explore the theory space around ΛCDM and let observations highlight which regions of this theory space are the most favored. The efforts for building models could then be focused to these particular regions. The difficult part there is that one has to deal with free functions of time, which are difficult to constrain with the limited observations that we have.

The goal of this paper is to try and see if, given the sensitivity of future surveys, one can approximate the complicated landscape of the arbitrary time dependences by a much simpler theory space, only given by a few parameters. We summarize our method in Fig. 1.

In Sec. II, we briefly review and expose the features of the EFT of DE that are relevant for our analysis. Then, in Sec. III, we present the way we are going to explore the theory space and how we are going to estimate the performance of simpler parametrizations. The results are then detailed in Sec. IV, and final conclusions are drawn in Sec. V.

II. FRAMEWORK

The EFT of DE formalism has been carefully reviewed in Ref. [15]. For our purposes, the key conclusion is that, assuming the background is fixed, the evolution of perturbations is, in principle, determined by five free functions of time. In Ref. [14] and later Ref. [15], those functions were expressed in a way that highlighted their effects on the theory space and are written as $\{\alpha_K, \alpha_B, \alpha_T, \alpha_M, \alpha_H\}$:

[1]More functions are needed if the weak equivalence principle is broken, i.e., dark matter and baryons are coupled to different metrics [9].

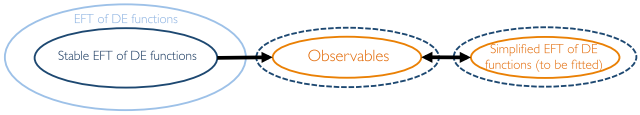

FIG. 1. Representation of the method used in this paper. We will compute observables (galaxy and weak lensing power spectra) from complex EFT of DE functions after imposing stability conditions. They will be fitted to simplified versions of these functions. Then, we will use model comparison tools to assess whether the complexity (i.e., the size of the circle) of the original functions is actually transferred to the observables or if simple functions are enough capture the physical features. In this diagram, this essentially corresponds to comparing the size of the dark blue and the orange circles. Moreover, we want the orange circle on the right to be the same size as the middle one; i.e., the simple functions have to explain the whole observable space.

(i) $\alpha_{\rm K}$ parametrizes the kinetic energy of the extra degree of freedom and is the simplest extension to GR. Setting all the other functions to zero will capture simple dark energy models (i.e., with no modifications to gravity except the presence of an extra fluid).
(ii) $\alpha_{\rm B}$ is linked to so-called braiding scalar-tensor models [18] in which part of the kinetic energy of the scalar is sourced through a coupling to gravity, resulting in deeper modifications of gravity.
(iii) $\alpha_{\rm T}$ controls the deviation of the speed of tensor perturbations from that of light, which is allowed when going outside of GR. It could, in principle, be measured independently using gravitational waves [19].
(iv) $\alpha_{\rm M}$ is nonzero when the Planck mass, denoted $M(t)$ and defined as the coupling between gravity waves and matter, is not constant in time. In scalar-tensor theories, this happens when the scalar field couples directly to the Ricci scalar.
(v) $\alpha_{\rm H}$ vanishes for theories that belong to the Horndeski class [10], in which terms with more than two derivatives are forbidden from the equations of motion. However, a proper interpretation of Ostrogradski's theorem [20] indicates that higher derivatives are not necessarily synonymous with instabilities. What is important is that the actual degrees of freedom, once constraint equations are solved, obey second-order differential equations. This is the case in theories dubbed beyond Horndeski [11–13] (see also Refs. [21–25]) and leads to $\alpha_{\rm H} \neq 0$.

The advantage of using this set of functions (instead of the original set of Refs. [6–8]) is that if any of them were measured to be nonzero it would directly point toward one specific aspect of modified gravity. For a shorthand notation, we will denote this set by $\{\alpha_{\rm X}\}$.

Using these functions, one can derive the modified Einstein equations as well as an evolution equation for the extra degree of freedom. If one further supplements them with the conservation of the matter stress-energy tensor, the system can be solved to obtain the evolution of a (linear) matter overdensity. However, even if the functions $\{\alpha_{\rm X}\}$ are taken to have simple and known time dependences, the system of equations can only be solved numerically. Different groups have developed codes in order to do so, such as EFTCAMB [26], Hi-Class [27], or COOP [28]. Here, for the sake of simplicity, we will look at the simpler case of the extreme quasistatic (EQS) limit, which is justified when looking at overdensities on scales much smaller than the sound horizon of the extra DOF [29]. To make this more quantitative, let us explicitly introduce the metric in Newtonian gauge (which is convenient for phenomenological studies). The line element reads

$$ds^2 = -(1+2\Phi)dt^2 + a(t)^2(1-2\Psi)d\vec{x}^2. \tag{1}$$

Since this analysis is limited to linear perturbations, it is easier to go to Fourier space. Taking the EQS means looking at wave numbers $k \gg c_s^{-1}aH$, where c_s is the speed of sound of the extra DOF (that can be expressed in terms of the $\{\alpha_{\rm X}\}$) and the Hubble rate is defined as $H \equiv \dot{a}/a$. We will also limit ourselves to the case $\alpha_{\rm H} = 0$ to keep expressions simpler. In this limit, one recovers a growth equation for matter overdensities $\delta_{\rm m}$ that is similar to that of GR, given by (omitting the explicit time dependences for brevity)

$$\ddot{\delta}_{\rm m} + 2H\dot{\delta}_{\rm m} = \frac{3}{2}\Omega_{\rm m}H^2\mu_{\rm eff}\delta_{\rm m}, \tag{2}$$

$$\mu_{\rm eff} \equiv (1+\alpha_{\rm T}+\beta_\xi^2), \tag{3}$$

where we have defined

$$\Omega_{\rm m} \equiv \frac{\rho_{\rm m}}{3H^2M^2}, \qquad \beta_\xi \equiv \frac{\sqrt{2}}{c_s\alpha^{1/2}}[\alpha_{\rm B}(1+\alpha_{\rm T})+\alpha_{\rm T}-\alpha_{\rm M}]. \tag{4}$$

$\alpha \equiv \alpha_{\rm K} + 6\alpha_{\rm B}^2$ is the total kinetic energy of the scalar field, and its speed of sound is given as

$$c_s^2 \equiv -\frac{2}{\alpha}\left\{(1+\alpha_{\rm B})\left[\frac{\dot{H}}{H^2}-\alpha_{\rm M}+\alpha_{\rm T}+\alpha_{\rm B}(1+\alpha_{\rm T})\right] + \frac{\dot{\alpha}_{\rm B}}{H}+\frac{3}{2}\Omega_{\rm m}\right\}. \tag{5}$$

Stability conditions impose that both $\alpha > 0$ (no-ghost condition; see Ref. [30]) and $c_s^2 > 0$ (no gradient instability), ensuring that β_ξ is real. Even in the absence of any anisotropic stress, modified gravity models do not have $\Phi = \Psi$ as for GR in the Newtonian gauge. This is important, as weak lensing measurements are sensitive to

the so-called lensing potential, $\Psi + \Phi$. In terms of the $\{\alpha_X\}$, this potential can be written as

$$\Phi + \Psi = -\frac{3a^2H^2}{k^2}\Omega_m \mu_{\rm light}\delta_m, \tag{6}$$

$$\mu_{\rm light} \equiv \frac{2 + \alpha_T + (\beta_\xi + \beta_B)\beta_\xi}{2}, \qquad \beta_B \equiv \frac{\sqrt{2}\alpha_B}{c_s \alpha^{1/2}}. \tag{7}$$

If $\alpha_T = \alpha_M = 0$, then one finds that $\Phi = \Psi$, but otherwise, they are different.

Thus, to get the power spectrum at a given redshift, one needs, in principle, the whole evolution of the $\{\alpha_X\}$. If we had perfect knowledge of the evolution of the matter field from high redshifts to today, one could create a fine binning in redshift and associate a parameter for each function in each bin. For realistic surveys, however, it would be better if those free functions of time could be fixed in terms of a few constant parameters. This is why a number of groups [14,31–34] have decided, for a first attempt, to parametrize the functions of time as proportional to $1 - \Omega_m$. Indeed, under the assumption of a spatially flat Universe, $\Omega_m = 1$ if the Universe contains only matter and is smaller if there are other components. Therefore, $1 - \Omega_m$ controls the density of what is causing the accelerated expansion of the Universe.[2] This is why it is pretty natural to assume that deviations to ΛCDM would trace this quantity.

Of course, the time evolution could be a more complicated function of $1 - \Omega_m$, and it could be different for every function $\{\alpha_X\}$. There have been attempts to see whether this simple parametrization reproduces known models, such as Galileons [35], with some indicating reasonable agreement [36] with others claiming the opposite [37]. Since it is not clear whether they probed the same part of the theory space, this is not necessarily a contradiction. However, Galileons are not necessarily representative of the full theory space that we are trying to explore. Nor are they the most motivated candidates from a cosmological point of view, having trouble with some observations such as void lensing [38] and the Integrated Sachs–Wolfe (ISW) effect [39] (see also Ref. [40] for a more detailed analysis). Therefore, even if simple parametrizations turned out to not be working very well for these models, that would not undoubtedly mean that they should be thrown away.

In this paper, we argue that whether a simple parametrization can reproduce the complete, detailed evolution of the $\{\alpha_X\}$ coming from complicated models is not the most relevant question. Indeed, it is not obvious the potential short time-scale features in the $\{\alpha_X\}$ are actually observable. For instance, their effect on the growth is integrated, as seen in Eq. (2), so one might guess that sharp features are smoothed out. Instead, we would rather see whether the difference between simple and complicated evolution of the $\{\alpha_X\}$ can actually be measured.

To try and answer this question, we will do the following: take the $\{\alpha_X\}$ to be random, different functions of time and compute the corresponding power spectra, for galaxies and weak lensing. Then, we will try and see if we can fit the observables using the simple parametrizations and minimizing the χ^2 for said observables. This differs from previous analyses in three major ways. First, because we take the functions to be random, the exploration of the theory space is not biased toward a specific model. Second, for each value of $\{\alpha_X\}$ today, we will take many different realizations of the random functions so that we can make quantitative statement about how often the parametrization fails. Finally, the comparison and fitting will be at the level of the observables, not of the functions $\{\alpha_X\}$ nor $\mu_{\rm eff,light}$, which are not directly measurable.

III. SETUP

We want to explore the theory space of the $\{\alpha_X\}$ and see if it can be approximated by a simple, finite-dimensional parameter space. To do so, we can start from a very large space, essentially mimicking the infinite-dimensional space, and see if the simple parametrization allows us to recover the features of this complex parameter space that are relevant for cosmological surveys, i.e., those conveyed to the observables.

Before detailing the exact procedure, let us note that, within the approximations that we have described in the previous section, particularly the EQS, only three functions $\{\alpha_B, \alpha_T, \alpha_M\}$ have an effect. We set $\alpha_H = 0$, and α_K does not appear in the equations. For each of the three remaining functions, we will parametrize the "true" theory space as

$$\alpha_X^{\rm true}(z) = \alpha_{X,0}(1+z)^{-q_X}\left(\frac{1 + \sum_{i=1}^{i_{\rm max}} n_{X,i} z^i}{1 + \sum_{i=1}^{i_{\rm max}} d_{X,i} z^i}\right), \tag{8}$$

where $X \in \{B, T, M\}$. We express the time variable as the redshift $z = a(t)^{-1} - 1$, and $\alpha_{X,0}$ is the value of α_X today ($z = 0$). The choice of the factor $(1+z)^{-q_X}$ is to ensure that α_X goes to zero in the past, because we want the effect of modified gravity to only become manifest in the late Universe, not during matter domination ($z \gg 1$). This is also a generic feature of Horndeski models, as pointed out in Ref. [37]. Finally, the last part of this function allows for complicated evolutions. The choice of a rational function and not of a polynomial is because typically the $\{\alpha_X\}$ are defined as ratios of functions that involve the extra degree of freedom (see, e.g., Ref. [15]). Moreover, this covers a larger portion of the theory space that we want to explore and does not exclude the possibility of divergent $\{\alpha_X\}$, just as expected from Ref. [15].

We have checked that this form can fit the case of k-essence [41], in which only α_K is nonzero, and goes as

[2]The density of radiation is negligible in the recent Universe, so it can safely be ignored from $1 - \Omega_m$.

TABLE I. The choice of (linear) priors on the parameters of Eq. (8). For the theory priors, we impose that both σ_8 and $\mu_{\rm light}\sigma_8$ are within 25% of the ΛCDM value.

$\alpha_{\rm X,0}$	$q_{\rm X}$	$\{d_{{\rm X},i}, n_{{\rm X},i}\}$	Theory priors
$[-1, 1]$	[2, 6]	$[-100, 100]$	$c_s^2\alpha > 0$ and $\lvert(\mu_{\rm light})\sigma_8/\sigma_8^{\Lambda\rm CDM} - 1\rvert < 0.25$

$1 - \Omega_{\rm m}$ [14]. It also works for more involved cases, such as Galileon models [42]. To check that, we numerically solved the full background equations,[3] computed the $\{\alpha_{\rm X}\}$, and fitted Eq. (8) to them. We found that with $i_{\rm max} = 8$ one could fit the $\{\alpha_{\rm X}\}$ from the Galileon models to better than 10^{-5} accuracy. We will thus assume this value from now on.

The procedure is then as follows. We first choose a triplet $\{\alpha_{\rm B,0}, \alpha_{\rm T,0}, \alpha_{\rm M,0}\}$ for $\alpha_{\rm X,0} \in [-1, 1]$. This is a way to enforce an observer's prior, excluding models potentially ruled out by current observations. For each triplet, we choose at random the three $\{q_{\rm X}\}$, between [2, 6], and the $6 \times i_{\rm max}$ parameters $\{d_{{\rm X},i}, n_{{\rm X},i}\}$ between $[-100, 100]$. If the corresponding $c_s^2\alpha$ computed from Eq. (5) crosses zero anytime between $z = 0$ and $z = z_{\rm ini} = 20$, we discard this realization. Otherwise, we compute the evolution of $\delta_{\rm m}$, setting the initial conditions in matter dominance ($z = z_{\rm ini}$). Since we choose our functions to decay, in principle, at least as $(1 + z)^{-2}$ for $z \gg 1$, their effect is negligible, and we have the usual solution $\delta_{\rm m}(z \gg 1) = (1 + z)^{-1}$. We summarize the choice of priors in Table I.

The final cut that we make on the theory space is that, for each redshift bin, we compute σ_8 for the matter power spectrum (its amplitude in a sphere of radius $8h/{\rm Mpc}$) and $\mu_{\rm light}\sigma_8$, the one associated to weak lensing. The current errors on σ_8 from redshift-space distortions and weak lensing are of order 15% [43,44]. Therefore, if the σ_8 and $\mu_{\rm light}\sigma_8$ that we find are not within 25% (to be conservative) of those computed in ΛCDM, we reject the realization. This is to be consistent with the fact that no deviation from ΛCDM has been observed. Then, we want to know if the observables produced with the complicated $\{\alpha_{\rm X}\}$ in Eq. (8) can be fitted with simple parametrizations. Within the representation of Fig. 1, this means checking that the two orange circles are the same size. To do this, we will fit the true model to given parametrizations by minimizing the χ^2 for the combination of two probes, galaxy clustering and weak lensing tomography, and then compute the associated Bayesian information criterion (BIC), defined as

$$\mathrm{BIC} \equiv \chi^2_{\rm min} + k \ln N, \tag{9}$$

with k the number of parameters to be fitted and N the number of data points. The last term is to penalize models with unnecessary complexity.

[3]Using a python script generously provided by Alexandre Barreira.

A. Simple parametrizations

The procedure described above will be applied to different parametrizations, with an increasing level of complexity; at the end, they will be compared to the true model, as well as each other:

(i) With a wCDM model (all the $\{\alpha_{\rm X}\} = 0$) and $w \in [-1.02, -0.92]$, using prior knowledge from distance measurements [45]. This is to check whether one really needs modified gravity or if dark energy could explain the observables.

(ii) With a parametrization given by

$$\alpha_{\rm X} = \alpha_{\rm X,0}\frac{1 - \Omega_{\rm m}}{1 - \Omega_{\rm m,0}}, \tag{10}$$

where $\Omega_{\rm m,0}$ is the current value of the density parameter "$\Omega_{\rm m}$." We will label it "$\Omega_{\rm m}$." This one has been commonly used in forecasting papers [14,31–34]. Note that there are two assumptions behind it: that all of the $\{\alpha_{\rm X}\}$ have the same time dependence and that time dependence is fixed.

(iii) With a parametrization given by

$$\alpha_{\rm X} = \alpha_{\rm X,0}(1 + z)^{-q}, \tag{11}$$

with the same q for all the $\{\alpha_{\rm X}\}$. We will label it "1i", for one index. Here, we relax the assumption of a fixed time dependence but keep all of the $\{\alpha_{\rm X}\}$ proportional to the same function.

(iv) With a parametrization given by

$$\alpha_{\rm X} = \alpha_{\rm X,0}(1 + z)^{-q_{\rm X}}, \tag{12}$$

with a different $q_{\rm X}$ for each $\alpha_{\rm X}$. We will label it "3i", for three indices. We have relaxed the two assumptions of the case $\Omega_{\rm m}$. We only impose that the functions have this simple redshift dependence, which gets negligible at high redshifts.

In every parametrization, the background is a wCDM, with w determined by the fitting procedure. More precisely, its range w is increased to $[-1.2, 0.8]$. This is to be conservative, since, in principle, a nonzero $\alpha_{\rm M}$ (i.e., a time-varying Planck mass) changes the expansion history, inducing degeneracies in the determination of w from distance measurements. Finally, the parameters $\{\alpha_{\rm X,0}\}$ are allowed to vary between $[-50, 50]$, and the indices $\{q_{\rm X}\}$ vary between [0, 6].

To compare with the true model, we need to compute its BIC. However, since we are just interested in quantifying whether the complexity of Eq. (8) is necessary, we will only keep the second term in Eq. (9), $k \ln N$. Note that, in principle, even if the Universe were given by Eq. (8), the measurements would have noise, which means that the BIC computed with the true model would also receive a $\chi^2_{\rm min}$ contribution (it would roughly be of order the number of measurements; see, e.g., Ref. [46]). This can only increase the BIC, so we deliberately choose not to include that term and focus on the second one to be extremely conservative. This is an irreducible theoretical floor for the BIC, which encodes the size of the theory space described by Eq. (8). In the context of Fig. 1, this is a proxy for the size of the dark blue circle.

B. Galaxy clustering

For galaxy clustering, we assume a spectroscopic redshift survey of 15000 squared degrees, sliced in eight equally populated redshift bins (we take the galaxy distribution as given by Ref. [47] with a limiting flux placed at 4×10^{-16} ergs^{-1} cm^{-2}) between $z = 0.5$ and $z = 2.1$, as in Ref. [32]. These characteristics are similar to those expected in DESI [3] or EUCLID [5]. We then compute the χ^2 for a model $\mathcal{M}$,

$$\chi^2_{\rm PS,\mathcal{M}} \equiv \sum_{k,i} [P_{\rm true}(k,z_i) - P_{\mathcal{M}}(k,z_i)]^2 \sigma^{-2}_{k,i},$$
$$\sigma^2_{k,i} \equiv 2N^{-1}_{k,i} P_{\rm true}(k,z_i)^2, \tag{13}$$

where $N_{k,i} \equiv \frac{k^2 V_i}{2\pi^2}\Delta k$ is the number of modes in a k bin $[k, k+\Delta k]$ for a redshift bin centered around z_i, the volume of which is $V_i = V(z_i)$. $P_{\rm true}(k,z)$ is the power spectrum at redshift z and wave number k, computed with a given realization of Eq. (8), and $P_{\mathcal{M}}$ is the one computed with a model $\mathcal{M}$, where the $\{\alpha_{\rm X}\}$ are given by wCDM or either one of Eqs. (10)–(12).

In the EQS approximation, the k dependence of the linear power spectrum is not modified by the deviations to ΛCDM. Thus, it drops out of the χ^2, and the sum over the k modes just gives an overall factor that depends only on the details of the survey—which sets $V(z_i)$—and on the maximum wave number in the analysis, $k_{\rm max}(z_i)$. The latter is chosen as the minimum between the linear scale and the scale where the shot noise starts to dominate. This guarantees that our linear description is consistent and that we can safely ignore the shot noise in $\sigma_{k,i}$.

In principle, the minimum wave number included in our analysis is set by the range of validity of the EQS. Typically, this means $k_{\rm min} \gg H_0^{-1}$, with the specific value depending on the $\{\alpha_{\rm X}\}$ (see Ref. [29] for more details). However, because of the scale independence of our modifications to the linear power spectrum, the signal to noise in a k bin goes as $k^2\Delta k$ and thus peaks close to $k_{\rm max}$. Therefore, the precise choice of $k_{\rm min}$ is irrelevant, as long as $k_{\rm min} \ll k_{\rm max}$, which is guaranteed for $k_{\rm min} \sim 10 H_0^{-1}$.

To simplify the analysis further, we will assume the same galaxy bias in every model so that it cancels out of Eq. (13). Moreover, we will not take into account redshift space distortions because theoretically they probes the same quantity, the linear growth, so that we do not expect differences in the final results.

C. Weak lensing

For weak lensing, we consider lensing tomography [48]. The angular cross-correlation spectra of the lensing cosmic shear for a set of galaxy redshift distributions $n_i(z)$ is given by

$$P^{\rm WL}_{ij}(\ell) = \frac{\ell}{4}\int_0^\infty \frac{dz}{H(z)} \frac{W_i(z) W_j(z)}{\chi^3(z)} k^3_\ell(z) P_{\Phi+\Psi}[z, k_\ell(z)], \tag{14}$$

where $\chi(z) \equiv \int_0^z dz/H(z)$ is the comoving distance and the lensing efficiency in each bin is given by

$$W_i(z) \equiv \chi(z) \int_z^\infty d\tilde{z} n_i(\tilde{z}) [\chi(\tilde{z}) - \chi(z)]/\chi(\tilde{z}), \tag{15}$$

with each galaxy distribution normalized to unity, $\int_0^\infty dz n_i(z) = 1$. Moreover, $P_{\Phi+\Psi}(k)$ is the power spectrum of $\Phi + \Psi$. Using Eq. (6), it is related to the matter power spectrum by

$$P_{\Phi+\Psi}(z,k) = \left(\frac{3a^2H^2\Omega_{\rm m}\mu_{\rm light}}{k^2} \frac{\delta_{\rm m}(z)}{\delta_{\rm m}(z=0)}\right)^2 P_0(k), \tag{16}$$

where $P_0(k)$ is the power spectrum at $z = 0$. Finally, we define $k_\ell(z) \equiv \ell/\chi(z)$ as the wave number that projects into the angular scale ℓ, which we will take to vary between [10, 1000], restricting to linear scales. Furthermore, we follow, e.g., Ref. [34] and assume a photometric survey of 15000 squared degrees in the redshift range $0 < z < 2.5$, with a redshift uncertainty $\sigma_z(z) = 0.05(1+z)$ and a galaxy distribution $n(z) \propto z^2 \exp[-(z/z_0)^{1.5}]$ [49], where $z_0 = z_m/\sqrt{2}$ and z_m is the median redshift, assumed to be $z_m = 0.9$ [50,51]. Then, we divide the survey into 12 equally populated redshift bins. For each bin i, we define the distribution $n_i(z)$ by convolving $n(z)$ with a Gaussian of which the dispersion is equal to the photometric redshift uncertainty $\sigma_z(z_i)$, z_i being the center of the ith bin (see also Refs. [52,53]). Adding a diagonal term to account for intrinsic ellipticity of galaxies (see, e.g., Ref. [54,55]), we find

$$C_{ij}(\ell) \equiv P^{\rm WL}_{ij}(\ell) + \delta^i_j \sigma^2_\epsilon \bar{n}_i^{-1}, \tag{17}$$

where $\bar{n}_i = 3600 \times (180/\pi)^2 n_\theta / N_{\rm bins}$ is the average number of galaxies per radian^2 per bin, assuming a total number

of galaxies per arcmin^2 $n_\theta = 30$ and $N_{\rm bins}$ equally populated bins. The intrinsic ellipticity is characterized by σ_e, which we take to be 0.22 (EUCLID-like characteristics; see, e.g., Ref. [34]). We then assume a Gaussian likelihood, with covariance given by

$$C_{ij}^{\rm true}(\ell) \equiv P_{ij}^{\rm WL,true}(\ell) + \delta_j^i \sigma_e^2 \bar{n}_i^{-1}, \tag{18}$$

so that the χ^2 is given by

$$\chi^2_{\rm WL,\mathcal{M}} \equiv f_{\rm sky} \sum_{\ell_{\rm min}}^{\ell_{\rm max}} \frac{2\ell+1}{2} \times {\rm Tr}[(C_\ell^{\mathcal{M}} - C_\ell^{\rm true}) \cdot (C_\ell^{\rm true})^{-1} \cdot (C_\ell^{\mathcal{M}} - C_\ell^{\rm true}) \cdot (C_\ell^{\rm true})^{-1}], \tag{19}$$

where $f_{\rm sky} = 0.36$, $l_{\rm min} = 10$, and $l_{\rm max} = 1000$. Contrarily to the case of galaxy clustering, the scale dependence of the power spectrum does not factor out of the χ^2. Thus, we need to fix $P_0(k)$ in Eq. (16). To do so, we use CAMB [56] to compute the power spectrum in ΛCDM at $z = 0$, $P_0^{\Lambda\rm CDM}$. Then, since the scale dependence is not changed in our scenario, we have

$$P_0^{\mathcal{M}}(k) = P_0^{\Lambda\rm CDM}(k)(\delta_{\rm m}^{\mathcal{M}}/\delta_{\rm m}^{\Lambda\rm CDM})^2(z=0), \tag{20}$$

where $\delta_{\rm m}^{\mathcal{M}}$ is the linear growth computed in the modified gravity model $\mathcal{M}$ and $\delta_{\rm m}^{\Lambda\rm CDM}$ the is the linear growth in ΛCDM.

IV. RESULTS

Even before trying to fit the parametrizations of Sec. III A, taking many realizations of Eq. (8) allows us to make general statements about the theory space itself, which we will explain in Sec. IV A. Then, we will go into the details of how the parametrizations perform in Sec. IV B. While for both sections the detailed and quantitative results depend on the exact form chosen in Eq. (8), the qualitative interpretation should not change too much, provided the form of $\{\alpha_{\rm X}\}$ is general enough.

A. From theory to observables

The first thing that should be noted is that imposing the stability condition $c_s^2\alpha > 0$ drastically reduces the size of the parameter space. We illustrate this in Fig. 2, where we summarize the distribution of evolutions for the $\{\alpha_{\rm X}\}$ for 10^4 realizations of three cases. The lines show where 95% of the curves lie. In dark purple, no conditions are imposed. In orange, we restrict realizations to $c_s^2\alpha > 0$. Only ∼0.15% of the functions satisfies this condition with linear priors on all the parameters in Eq. (8). Finally, in light green, we restrict to $c_s^2\alpha > 0$ and to having σ_8 and $\mu_{\rm light}\sigma_8$ within 25% of the ΛCDM value, to be consistent with past surveys, which represents ∼0.1% of the functions. For comparison, we plot also the cases in which the $\{\alpha_{\rm X}\}$ are given by Eq. (10) (black dotted-dashed curves) and by a quintic Galileon model (red dashed curves) with $\{c_2 = 3.8, c_3 = 2, c_4 = -1.3\times10^{-3}, c_5 = -4.7\times10^{-1}, c_g = 0.0, c_0 = 0, x_i = 2.8\times10^{-14}\}$ in the notation of Ref. [42], which yields the same set $\{\alpha_{\rm B,0}, \alpha_{\rm T,0}, \alpha_{\rm M,0}\} = \{-0.3, 1, -0.9\}$.

One can see that already the condition $c_s^2\alpha > 0$ significantly reduces the parameter space. It also makes the functions much smoother than the naive expectation. $\alpha_{\rm B}$ is somewhat special; it enters in a complicated, nonlinear way (it is also the only function that appears with a derivative) in c_s^2, and imposing $c_s^2\alpha > 0$ is not as constraining as for the other parameters; see the top right panel of Fig. 2. On the other hand, the same argument means that wildly varying $\alpha_{\rm B}$ does not necessarily lead to strong features in $\mu_{\rm eff}$, as seen in the bottom left panel of Fig. 2.

To each point $\{\alpha_{\rm B,0}, \alpha_{\rm T,0}, \alpha_{\rm M,0}\}$ is associated $n_{\rm runs} = 200$ random realizations of Eq. (8), which all satisfy $c_s^2\alpha > 0$ for the whole redshift range we consider. For each realization, we compute the matter growth as well as lensing potential, in order to get the galaxy and weak lensing power spectra. The second thing that we notice here is that, even if the complex evolution of the $\{\alpha_{\rm X}\}$ leads to strongly varying $\mu_{\rm eff}$ and $\mu_{\rm light}$, this is not completely transferred to the observables, as seen in Fig. 3.

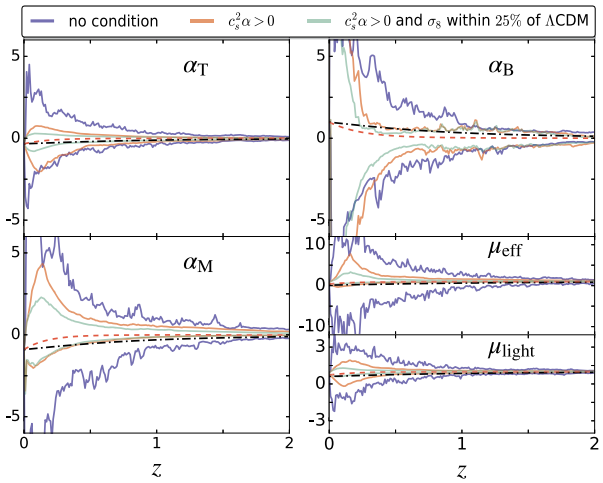

FIG. 2. Comparisons of the distribution of redshift evolution of $\alpha_{\rm T}$ (*top left*), $\alpha_{\rm B}$ (*top right*), $\alpha_{\rm M}$ (*bottom left*), and $\mu_{\rm eff}$ and $\mu_{\rm light}$ (*bottom right*) for $\{\alpha_{\rm B,0}, \alpha_{\rm T,0}, \alpha_{\rm M,0}\} = \{-0.3, 1, -0.9\}$. The lines delimit where 95% of the curves resides. In dark purple is the case in which there is no restriction on $c_s^2\alpha$. In orange is the parameters taken only if the corresponding $c_s^2\alpha$ is positive. Finally, in light green is the case in which $c_s^2\alpha > 0$ and σ_8, as well as $\mu_{\rm light}\sigma_8$, are within 25% of the ΛCDM value. The black dotted-dashed lines correspond to the $\{\alpha_{\rm X}\}$ evolving according to Eq. (10), while the red dashed lines are for a quintic Galileon model with a the same set $\{\alpha_{\rm X,0}\}$, fixed by the model parameters (see the main text for details).

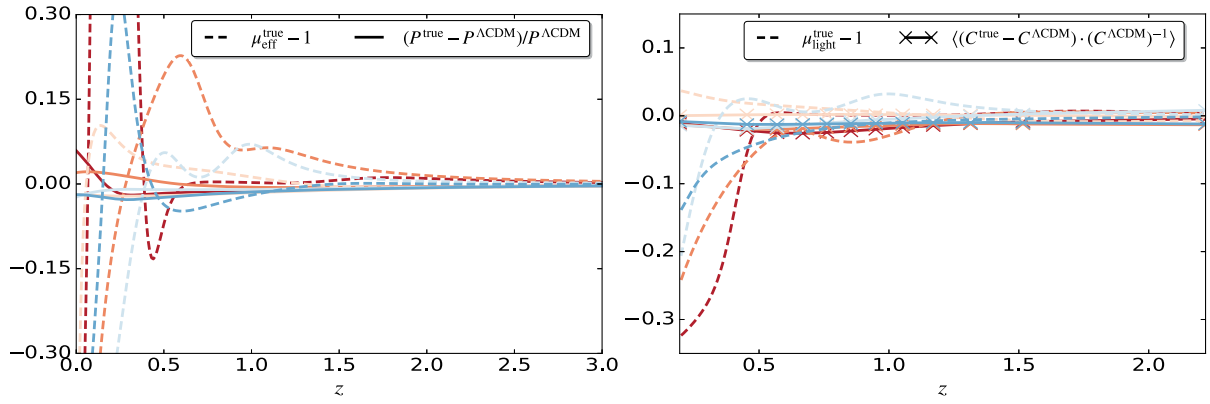

FIG. 3. We plot the relative difference of μ_{eff} and μ_{light} w.r.t. their LCDM values (dashed) compared to the relative difference in the corresponding observables (same color, full line), respectively the galaxy power spectrum and the C_{ij} averaged over ℓ. The five colors are for five different random realizations of Eq. (8). For weak lensing, the crosses indicate the center of the redshift bins. While $\mu_{\rm eff}$ and $\mu_{\rm light}$ vary on a short time scale and by significant amounts (more than 200% for $\mu_{\rm eff}$), the observables are much smoother, and the deviations are much smaller.

This is because to get the growth one has to integrate Eq. (2), which means variations in $\mu_{\rm eff}$ are not directly transferred to variations in the power spectrum. For weak lensing, $\mu_{\rm light}$ appears explicitly, and one might think that the effects should be more apparent. However, to get the lensing power spectrum in Eq. (14), one has to integrate over the window functions, which also smooths the variations in $\mu_{\rm light}$. To estimate the deviations in the weak lensing power spectra, we use the quantity

$$\langle(C^{\rm true}-C^{\mathcal{M}})\cdot(C^{\rm true})^{-1}\rangle(z_i) \equiv \frac{\sum_\ell[(C_\ell^{\rm true}-C_\ell^{\mathcal{M}})\cdot(C_\ell^{\rm true})^{-1}]_{ii}}{l_{\rm max}-l_{\rm min}}, \quad (21)$$

where z_i is the middle of the redshift bin i.

Schematically, what we have explained in this section is the left half of Fig. 1: the full space of functions (light blue) is larger than the one of stable functions (dark blue), which in turn is larger than the space of observables (orange). To explain the other half of that figure, we will try and fit the simple parametrizations of Sec. III A to the observables.

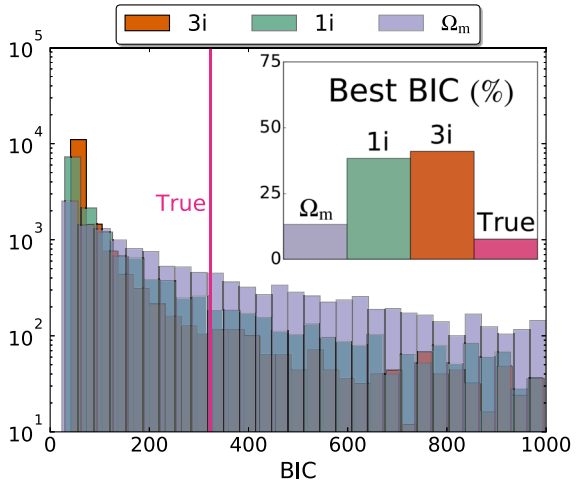

FIG. 4. Histogram of the BIC values for "$\Omega_{\rm m}$" (light purple), "1i" (green), and "3i" (dark orange), compared to the true value (pink line). The last one corresponds to a perfect fit $\chi^2=0$ with Eq. (8) but is penalized in the BIC due to its high number of parameters. Most (93%) of the time, at least one simpler model has a significantly lower BIC (ΔBIC <-10) than true, meaning it is preferred over the complex model. In the corner, we show the percentage of times when a given model has the lowest BIC.

B. Fitting the observables

Here, we minimize $\chi^2_{\mathcal{M}}\equiv\chi^2_{\rm WL,\mathcal{M}}+\chi^2_{\rm PS,\mathcal{M}}$, assuming the model $\mathcal{M}$ is given by either wCDM, the parametrization "$\Omega_{\rm m}$", or the parametrizations "1i" and "3i"as detailed in Sec. III A. From there, we can compute the BIC (9) and see which model is favored (the one with the lowest BIC). We show the results in Fig. 4, where we have restricted our analysis to cases in which the probability of an observed χ^2 being larger than $\chi^2_{\rm min,}w$CDM is smaller than 1%. This is to focus on cases that would lead to a detection of modified gravity, not simply a different equation of state for dark energy.

For most realizations, the simple parametrizations do better than the full model (8) in terms of the BIC. Having a lower BIC does not necessarily mean being a good fit. For those with a BIC lower than the true model's, however, one finds that they are always a reasonable fit to the observables.[4] Quantitatively, we find that, compared to the true model, "$\Omega_{\rm m}$", in light purple, is highly favored (ΔBIC <-10) 54%

[4]We have about 360 measurement points in our analysis.

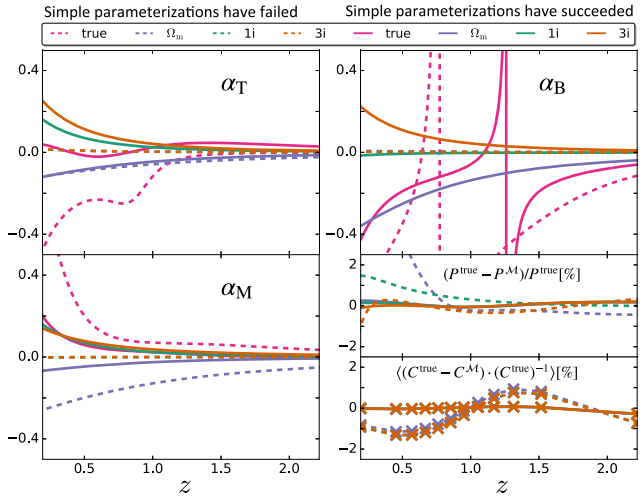

FIG. 5. Evolution of the $\{\alpha_X\}$ as a function of redshift for the true model (pink), "Ω_m" (purple), "1i" (green), and "3i" (orange). The dashed lines represent a case in which the simple parametrizations all failed at reconstructing the observables, while they all succeeded for the full lines. The bottom right panel shows the relative difference in the observables between the simple models and the true ones in a percentage. The crosses indicate the center of the redshift bins in the weak lensing measurement.

of the time, and for "1i" (green) this rises to 78% and for "3i" to 86% (dark orange). That is to say, the high complexities of the $\{\alpha_X\}$ are not transferred into the observables, at least at the sensitivity level of next-generation surveys. As a consequence, simple parametrizations are able to capture the behavior of modified gravity in the galaxy and weak lensing power spectra. Note that when doing the analysis with the galaxy power spectrum only then "Ω_m" is doing the best job 50% of the time. Adding lensing makes it harder to fit both observables with this fixed time dependence, making "3i" more adequate.

One could rightfully argue that "3i" comes out as the best parametrization because of the exact form of Eq. (8), which has the same factor $(1+z)^{-q_X}$. This is certainly true, but this adds to our argument that short time-scale variations—encoded in the rational function of Eq. (8)—are not observable, only smooth behaviors can be measured.

We show in Fig. 5 the evolution of the $\{\alpha_X\}$ as well as the relative difference in the power spectrum[5] and C_ℓ [given in Eq. (21)] for the different models $\mathcal{M}$, in two cases. With dashed lines, we show a case in which the simple parametrizations fail at reproducing the observables (all the $\Delta\text{BIC}_{\mathcal{M}-\text{true}} > 10$), and in full lines, we show a case in which they succeed (all the $\Delta\text{BIC}_{\mathcal{M}-\text{true}} < -10$).

As in Fig. 3, the strong features in the $\{\alpha_X\}$ are much smoother in the observables. In the successful case, in which α_T exhibits sizeable variations (top left panel), the observables are well reproduced by the smooth $\{\alpha_X\}$ of the simple parametrizations (bottom right panel). As we have noted after Fig. 2, the effect of α_B on the observables is not as simple as for the other functions, meaning that very complicated evolution such as the ones on the top right panel of Fig. 5 are not problematic for fitting simple parametrizations to observables. In the successful case for α_M, note that, indeed, the "1i" and "3i" capture its general behavior quite well but miss the short time-scale variations. For the bottom right panels, the three curves for the successful case are on top of each other and have a relative difference with the true observables that is less 0.3%.

V. DISCUSSION AND CONCLUSIONS

The possibility of an additional degree of freedom in gravity opens a vast theory space, described conveniently at the level of linear perturbations within the framework of the EFT of DE [15]. Formally, this theory space is infinite, as it depends on free functions of time $\{\alpha_X(z)\}$, not parameters. Therefore, it is not clear at first sight how one can use the EFT of DE to constrain modified gravity in upcoming surveys. In this article, we explored whether approximating this infinte-dimensional space by a finite one is sufficient to describe observables. This way,cosmological analyses can be reduced to actual parameters, not functions of redshift.

One approach that has been used in previous studies was to explore specific models, in which the $\{\alpha_X\}$ are derived from the evolution of the background field and the parameters of the model. Their evolution is thus known, and one can try to see whether they can be approximated by simple functions that one could then use as templates for analyzing data. While, in principle, this is certainly a promising way to go, we see it as limited in the context of modified gravity. The main reason is that, up to now, these studies have only focused on a small number of models, and a small number of parameters within those models, leading to contradicting results [36,37]. The problem is that, since there are no outstanding candidates for modified gravity, there is no reason to choose one particular model over another. Therefore, one should explore the whole model space (e.g., that of Horndeski theories [10]).[6] This is similar to what has been done at the level of the background expansion in Refs. [57,58]. However, this approach does not take full advantage of the powerful potential of EFT of DE to explore the large theory space systematically.

Thus, rather than explore the models, we take a more agnostic approach and directly explore the $\{\alpha_X\}$. To do so, we choose a convoluted form for their time dependence, Eq. (8), which allows a vast range of different evolutions. We have checked it can reproduce known models such as

[5]This is shown as a function of z and not k because the scale dependence is not modified in our approach.

[6]This would be a good first step, but as recent developments have shown [21–25], it is not clear Horndeski is the full picture of scalar-tensor theories.

the k-essence [41] and Galileons [35] to better than 10^{-5} accuracy.

The first thing that we notice is that the function space is actually smaller than expected because the $\{\alpha_X\}$ must obey stability conditions (namely, a positive kinetic term and positive sound speed). This drastically reduces the number of possible functions, by about a factor of 400 [with our uniform priors on the parameters of Eq. (8)]. This can be visualized in Fig. 2. If we then propagate the complex evolution of the $\{\alpha_X\}$ to the matter growth and lensing, one can see in Fig. 3 that strong variations in the $\{\alpha_X\}$ lead to strong variations in the modified gravitational couplings $\mu_{\rm eff}$ and $\mu_{\rm light}$ but that those variations are damped when looking at observables. This is one of the key points of this paper; it seems difficult to have access to short time variations of the $\{\alpha_X\}$ because observables are not very sensitive to them. Going back to the schematic representation of Fig. 1, this shows that the orange circle is indeed smaller than the dark blue one. Therefore, we anticipate that it is legitimate to use simple parametrizations to look for deviation to GR, even though they are much smoother than one might expect from models.

This is what we explore in the rest of the article. We compare how three different parametrizations could reproduce observables coming from a theory with complicated $\{\alpha_X\}$. In the first one, dubbed "Ω_m", all the $\{\alpha_X\}$ are proportional to $1-\Omega_m$, a common choice in the literature. For the second one, referred to as "1i", all of the $\{\alpha_X\}$ are proportional to the same function $(1+z)^{-q}$, where q is allowed to vary between $[0, 6]$. Finally, the last one, called "3i", allows for more freedom, each $\{\alpha_X\}$ being proportional to $(1+z)^{-q_X}$, with a different index $\in [0, 6]$ for each function. The functions $\{\alpha_X\}$ with those parametrizations do not exhibit sharp features, but since those are not observable, they can still be used to fit the galaxy and weak lensing power spectra rather well. In a sense, the complexity in Eq. (8) is not demanded by the observables because we cannot have access to it and therefore it is not relevant (at least naively, with the sensitivity of future experiments). To classify the performance of models while penalizing unnecessary complexity, we choose to use the BIC.

The results are shown in Fig. 4. Each parametrization is compared to the true case, i.e., the original model governed by Eq. (8), which fits the data perfectly but introduces 18 parameters for each $\{\alpha_X\}$. In 93% of the cases, one of the three simple parametrizations has a lower BIC, meaning the data do not need the introduction of the full complexity of Eq. (8). Our results show that, even though very high complexity is not necessary, taking all of the $\{\alpha_X\}$ with the same time dependence might be too simplistic. The model that performed best is the one with two parameters to describe each $\{\alpha_X\}$: an amplitude and power-law index.

The quantitative results of Fig. 4 are dependent on the exact form of Eq. (8) and the choice of the priors on the parameters. However, the fact that short time-scale variations of the $\{\alpha_X\}$ are not observables is more robust. This is also the case when using a rational function of $N=-\log[1+z]$ instead of z in Eq. (8) while increasing the prior on $\{d_{X,i}, n_{X,i}\}$ to $[-10^4, 10^4]$. This can reproduce known models to better than 10^{-5} as well, and the qualitative behavior described in Sec. IV A is very similar. There are some differences, for example, the number of stable functions represents ∼0.4% of all functions instead of ∼0.2% in Sec. IV A. The differences in the actual numbers of Sec. IV B (e.g., those of Fig. 4) are more minor: "Ω_m" does better than true 55% of the time instead of 54%, "1i" does better 83% of the time instead of 78%, and "3i" does better 90% of the time instead of 86%.

We have focused here on how well parametrizations can fit complex models, and we did not say much about actually constraining the $\{\alpha_X\}$. Indeed, with our simple approach in the EQS limit, the degeneracies are too strong to be broken with only galaxy clustering and weak lensing, as noted already in Ref. [32]. Therefore, the constraints would not really be meaningful. To get a sense, however, one can look at a simplified case in which α_M is fixed to zero. The degeneracies are not as strong in this case, and one can use Monte Carlo Markov chains (with only $\{\alpha_{X,0}, q_X\}$ as free parameters) to forecast the constraints, assuming a wCDM fiducial with $w=-0.95$. With "Ω_m", we get $\sigma(\alpha_X)\sim 0.03$. With "1i", this number is about ten times larger, and "3i" (which is rather "2i" here) gives results comparable to "1i". Thus, the constraints do degrade, but not by many orders of magnitude. It would be interesting to see how these numbers change with a more comprehensive analysis, such as the one with Hi-Class [27]. Indeed, this code uses the full equations (no quasistatic approximation) so that Ref. [33] was able to put constraints on all the $\{\alpha_X\}$. The authors used a parametrization similar to Ω_m (but with an additional constant parameter) as well as more complicated time dependences.

The optimal way to parametrize the functional freedom of the EFT of DE remains to be determined. We have shown that using simple parametrizations should do an adequate job. Another way to go could be to assign a different value to the $\{\alpha_X\}$ in each redshift bins. However, in that case, it is not clear how to enforce the stability conditions. Moreover, this would bring a very large number of parameters, which would considerably weaken the constraints, although one could use a principal component analysis (PCA) approach to extract the most constrained directions in the parameter space (see, e.g., Ref. [34]). The advantage of the three parametrizations that we explored here is that they are simple and somewhat physically motivated; the effects go to zero in matter domination. Plenty of other functions satisfy those two criteria, and we leave for future work a more comprehensive investigation.

ACKNOWLEDGMENTS

It is a pleasure to thank Alexandre Barreira, Phil Bull, Olivier Doré, Janina Renk, Filippo Vernizzi, and Miguel

Zumalacárregui for fruitful discussions and useful comments. Part of the research described in this paper was carried out at the Jet Propulsion Laboratory, California Institute of Technology, under a contract with the National Aeronautics and Space Administration. This research is partially supported by National Aeronautics and Space Administration (NASA) ROSES ATP 14-ATP14-0093 grant. U.S. Government sponsorship acknowledged.

[1] D. Spergel *et al.* (WFIRST Collaboration), Wide-Field Infra-Red Survey Telescope-Astrophysics Focused Telescope Assets WFIRST-AFTA Final Report, arXiv:1305.5422.
[2] P. A. Abell *et al.* (LSST Science and LSST Project Collaborations), LSST Science Book, Version 2.0, arXiv:0912.0201.
[3] A. Aghamousa *et al.* (DESI Collaboration), The DESI Experiment Part I: Science, Targeting, and Survey Design, arXiv:1611.00036.
[4] O. Doré *et al.*, Cosmology with the SPHEREX All-Sky Spectral Survey, arXiv:1412.4872.
[5] R. Laureijs *et al.* (EUCLID Collaboration), Euclid Definition Study Report, arXiv:1110.3193.
[6] G. Gubitosi, F. Piazza, and F. Vernizzi, The effective field theory of dark energy, J. Cosmol. Astropart. Phys. 02 (2013) 032,
[7] J. K. Bloomfield, É. É. Flanagan, M. Park, and S. Watson, Dark energy or modified gravity? An effective field theory approach, J. Cosmol. Astropart. Phys. 08 (2013) 010.
[8] J. Gleyzes, D. Langlois, F. Piazza, and F. Vernizzi, Essential building blocks of dark energy, J. Cosmol. Astropart. Phys. 08 (2013) 025.
[9] J. GleyzesD. Langlois, M. Mancarella, and F. Vernizzi, Effective theory of interacting dark energy, J. Cosmol. Astropart. Phys. 08 (2015) 054.
[10] G. W. Horndeski, Second-order scalar-tensor field equations in a four-dimensional space, Int. J. Theor. Phys. **10**, 363 (1974).
[11] M. Zumalacárregui and J. Garca-Bellido, Transforming gravity: From derivative couplings to matter to second-order scalar-tensor theories beyond the Horndeski Lagrangian, Phys. Rev. D **89**, 064046 (2014).
[12] J. Gleyzes, D. Langlois, F. Piazza, and F. Vernizzi, Healthy Theories Beyond Horndeski, Phys. Rev. Lett. **114**, 211101 (2015).
[13] J. Gleyzes, D. Langlois, F. Piazza, and F. Vernizzi, Exploring gravitational theories beyond Horndeski, J. Cosmol. Astropart. Phys. 02 (2015) 018.
[14] E. Bellini and I. Sawicki, Maximal freedom at minimum cost: linear large-scale structure in general modifications of gravity, J. Cosmol. Astropart. Phys. 07 (2014) 050.
[15] J. Gleyzes, D. Langlois, and F. Vernizzi, A unifying description of dark energy, Int. J. Mod. Phys. D **23**, 1443010 (2014).
[16] M. Lagos, T. Baker, P. G. Ferreira, and J. Noller, A general theory of linear cosmological perturbations: scalar-tensor and vector-tensor theories, J. Cosmol. Astropart. Phys. 08 (2016) 007.
[17] M. Lagos and P. G. Ferreira, A general theory of linear cosmological perturbations: Bimetric theories, J. Cosmol. Astropart. Phys. 01 (2017) 047.
[18] C. Deffayet, O. Pujolàs, I. Sawicki, and A. Vikman, Imperfect dark energy from kinetic gravity braiding, J. Cosmol. Astropart. Phys. 10 (2010) 026.
[19] D. Bettoni, J. M. Ezquiaga, K. Hinterbichler, and M. Zumalacárregui, Speed of gravitational waves and the fate of scalar-tensor gravity, Phys. Rev. D **95**, 084029 (2017).
[20] R. P. Woodard, Avoiding dark energy with 1/r modifications of gravity, Lect. Notes Phys. **720**, 403 (2007).
[21] C. Deffayet, G. Esposito-Farese, and D. A. Steer, Counting the degrees of freedom of generalized Galileons, Phys. Rev. D **92**, 084013 (2015).
[22] D. Langlois and K. Noui, Degenerate higher derivative theories beyond Horndeski: Evading the Ostrogradski instability, J. Cosmol. Astropart. Phys. 02 (2016) 034.
[23] D. Langlois and K. Noui, Hamiltonian analysis of higher derivative scalar-tensor theories, J. Cosmol. Astropart. Phys. 07 (2016) 016.
[24] J. B. Achour, D. Langlois, and K. Noui, Degenerate higher order scalar-tensor theories beyond Horndeski and disformal transformations, Phys. Rev. D **93**, 124005 (2016).
[25] M. Crisostomi, M. Hull, K. Koyama, and G. Tasinato, Horndeski: Beyond, or not beyond?, J. Cosmol. Astropart. Phys. 03 (2016) 038.
[26] B. Hu, M. Raveri, N. Frusciante, and A. Silvestri, Effective field theory of cosmic acceleration: An implementation in CAMB, Phys. Rev. D **89**, 103530 (2014).
[27] M. Zumalacárregui, E. Bellini, I. Sawicki, J. Lesgourgues, and P. G. Ferreira, hi_class: Horndeski in the cosmic linear anisotropy solving system, J. Cosmol. Astropart. Phys. 08 (2017) 019.
[28] G. D'Amico, Z. Huang, M. Mancarella, and F. Vernizzi, Weakening gravity on redshift-survey scales with kinetic matter mixing, J. Cosmol. Astropart. Phys. 02 (2017) 014.
[29] I. Sawicki and E. Bellini, Limits of quasistatic approximation in modified-gravity cosmologies, Phys. Rev. D **92**, 084061 (2015).
[30] F. Sbisà, Classical and quantum ghosts, Eur. J. Phys. **36**, 015009 (2015).
[31] L. Perenon, F. Piazza, C. Marinoni, and L. Hui, Phenomenology of dark energy: general features of large-scale perturbations, J. Cosmol. Astropart. Phys. 11 (2015) 029.
[32] J. Gleyzes, D. Langlois, M. Mancarella, and F. Vernizzi, Effective theory of dark energy at redshift survey scales, J. Cosmol. Astropart. Phys. 02 (2016) 056.
[33] D. Alonso, E. Bellini, P. G. Ferreira, and M. Zumalacárregui, The observational future of cosmological scalar-tensor theories, Phys. Rev. D **95**, 063502 (2017).
[34] S. Casas *et al.*, Linear and non-linear Modified Gravity forecasts with future surveys, arXiv:1703.01271.

[35] C. Deffayet, G. Esposito-Farese, and A. Vikman, Covariant Galileon, Phys. Rev. D **79**, 084003 (2009).
[36] J. Renk, M. Zumalacarregui, and F. Montanari, Gravity at the horizon: On relativistic effects, CMB-LSS correlations and ultra-large scales in Horndeski's theory, J. Cosmol. Astropart. Phys. 07 (2016) 040.
[37] E. V. Linder, Challenges in connecting modified gravity theory and observations, Phys. Rev. D **95**, 023518 (2017).
[38] A. Barreira, M. Cautun, B. Li, C. M. Baugh, and S. Pascoli, Weak lensing by voids in modified lensing potentials, J. Cosmol. Astropart. Phys. 08 (2015) 028.
[39] A. Barreira, B. Li, C. M. Baugh, and S. Pascoli, The observational status of Galileon gravity after Planck, J. Cosmol. Astropart. Phys. 08 (2014) 059.
[40] J. Renk *et al.*, Galileon Gravity in Light of ISW, CMB, BAO and H_0 data, arXiv:1707.02263.
[41] C. Armendariz-Picon, V. F. Mukhanov, and P. J. Steinhardt, A Dynamical Solution to the Problem of a Small Cosmological Constant and Late Time Cosmic Acceleration, Phys. Rev. Lett. **85**, 4438 (2000).
[42] S. Appleby and E. V. Linder, The paths of gravity in Galileon cosmology, J. Cosmol. Astropart. Phys. 03 (2012) 043.
[43] E. Macaulay, I. K. Wehus, and H. K. Eriksen, Lower Growth Rate from Recent Redshift Space Distortion Measurements than Expected from Planck, Phys. Rev. Lett. **111**, 161301 (2013).
[44] M. Kilbinger, Cosmology with cosmic shear observations: a review, Rep. Prog. Phys. **78**, 086901 (2015).
[45] Aubourg *et al.*, Cosmological implications of baryon acoustic oscillation measurements, Phys. Rev. D **92**, 123516 (2015).
[46] L. Verde, Statistical methods in cosmology, Lect. Notes Phys. **800**, 147 (2010).
[47] J. E. Geach *et al.*, Empirical H-alpha emitter count predictions for dark energy surveys, Mon. Not. R. Astron. Soc. **402**, 1330 (2010).
[48] W. Hu, Power spectrum tomography with weak lensing, Astrophys. J. **522**, L21 (1999).
[49] I. Smail, R. S. Ellis, and M. J. Fitchett, Gravitational lensing of distant field galaxies by rich clusters: I. Faint galaxy redshift distributions, Mon. Not. R. Astron. Soc. **270**, 245 (1994).
[50] A. Amara and A. Refregier, Optimal surveys for weak lensing tomography, Mon. Not. R. Astron. Soc. **381**, 1018 (2007).
[51] L. Amendola *et al.* (Euclid Theory Working Group Collaboration), Cosmology and fundamental physics with the Euclid satellite, Living Rev. Relativ. **16**, 6 (2013).
[52] T. Giannantonio, C. Porciani, J. Carron, A. Amara, and A. Pillepich, Constraining primordial non-Gaussianity with future galaxy surveys, Mon. Not. R. Astron. Soc. **422**, 2854 (2012).
[53] L. Amendola, V. Pettorino, C. Quercellini, and A. Vollmer, Testing coupled dark energy with next-generation large-scale observations, Phys. Rev. D **85**, 103008 (2012).
[54] B. Joachimi, P. Schneider, and T. Eifler, Analysis of two-point statistics of cosmic shear. 3. Covariances of shear measures made easy, Astron. Astrophys. **477**, 43 (2008).
[55] M. Takada and B. Jain, The impact of non-Gaussian errors on weak lensing surveys, Mon. Not. R. Astron. Soc. **395**, 2065 (2009).
[56] A. Lewis, A. Challinor, and A. Lasenby, Efficient computation of CMB anisotropies in closed FRW models, Astrophys. J. **538**, 473 (2000).
[57] D. J. E. Marsh, P. Bull, P. G. Ferreira, and A. Pontzen, Quintessence in a quandary: Prior dependence in dark energy models, Phys. Rev. D **90**, 105023 (2014).
[58] M. Raveri *et al.*, Priors on the effective Dark Energy equation of state in scalar-tensor theories, arXiv:1703.05297.